Supplementary Information

Layered carbon nitride bulk as a versatile cathode material for fast ion batteries

Jiaqi Zhang,[a] Jiaxin Jiang,[a] Hongyan Guo,[*a] Xiaowei Sheng,[a] Weiyi Wang,[b] Zhiwen Zhuo[*b] and Ning Lu[*a]

[a]Anhui Province Key Laboratory for Control and Applications of Optoelectronic Information Materials, Key Laboratory of Functional Molecular Solids Ministry of Education, and Department of Physics, Anhui Normal University, Wuhu, Anhui 241000, China

[b]Hefei National Research Center for Physical Sciences at the Microscale, University of Science and Technology of China, 96 Jinzhai Rd., Hefei 230026, China

[*]E-mail: hyguowd@ahnu.edu.cn; zhuozw@ustc.edu.cn; luning@ahnu.edu.cn

Table of Contents

AB and AA’ stacking

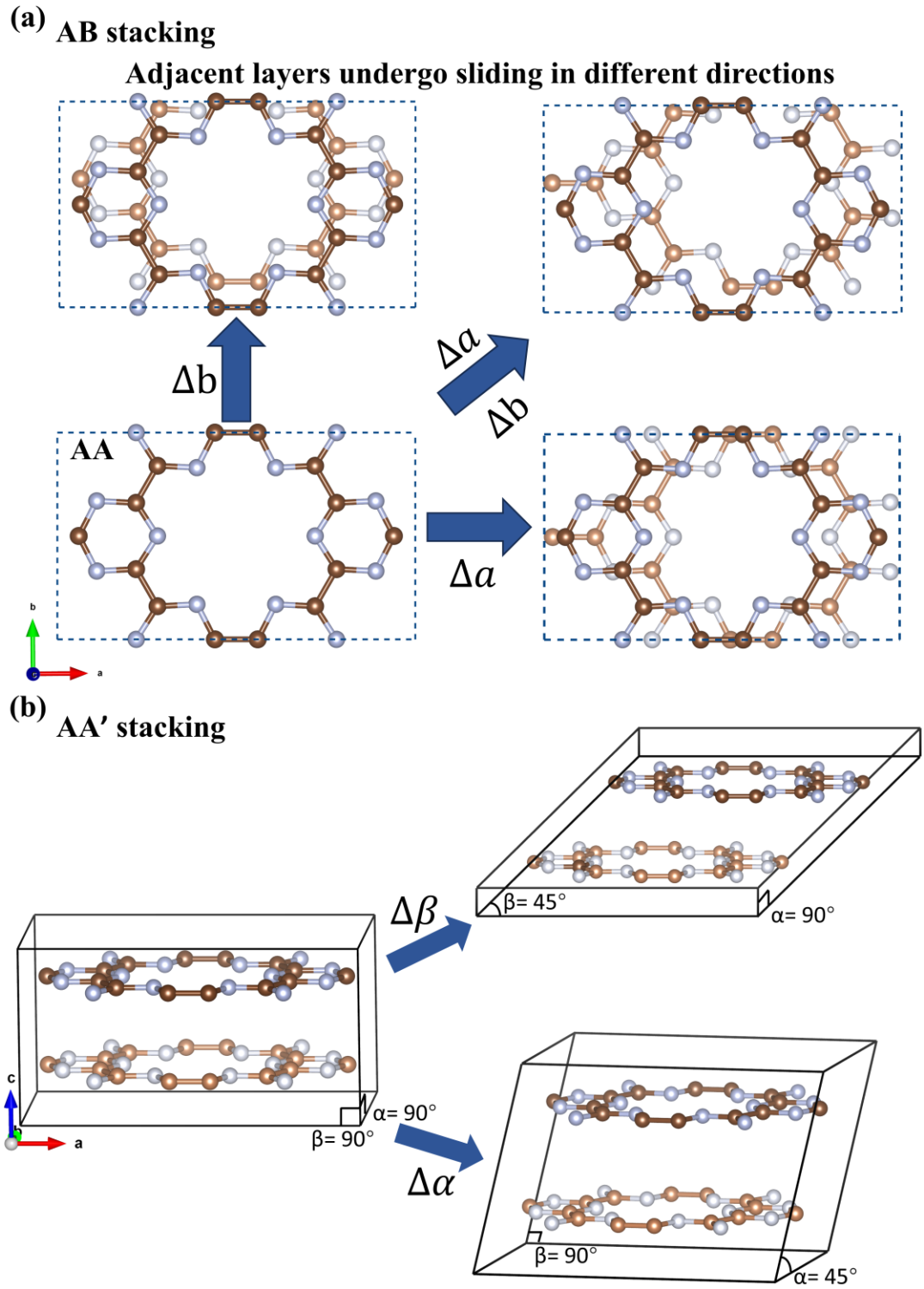

Fig. S1 Schematic Diagram of AB Stacking (a) and AA’ Stacking (b).

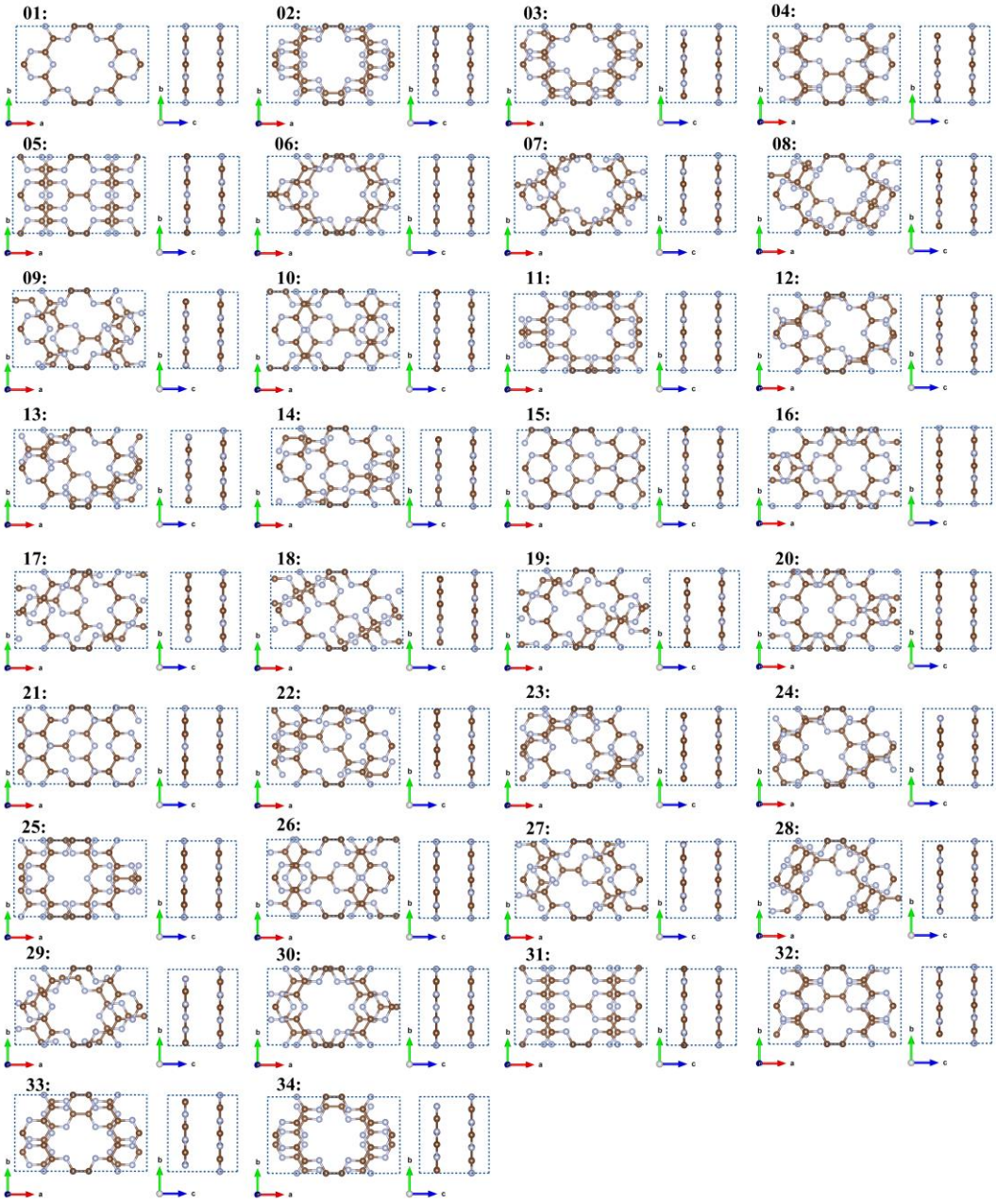

Fig. S2 Different configuration of vdW-CN with different periodic AB stacking for structure optimization. The dash lines indicate the lattice boundary of the 3D structure cell here.

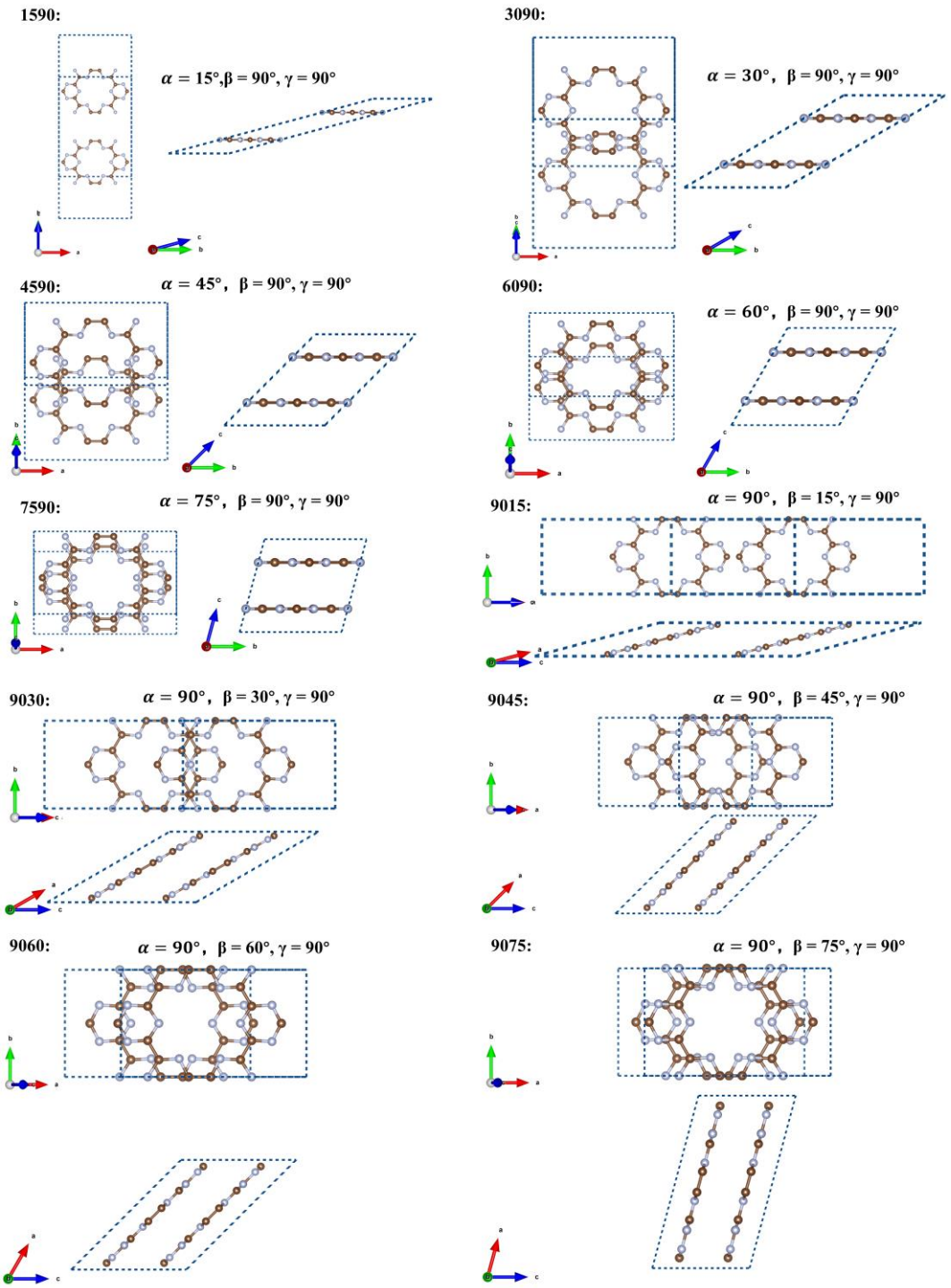

Fig. S3 Different configuration of vdW-CN with different periodic AA' stacking for structure optimization. The dash lines indicate the lattice boundary of the 3D structure cell here.

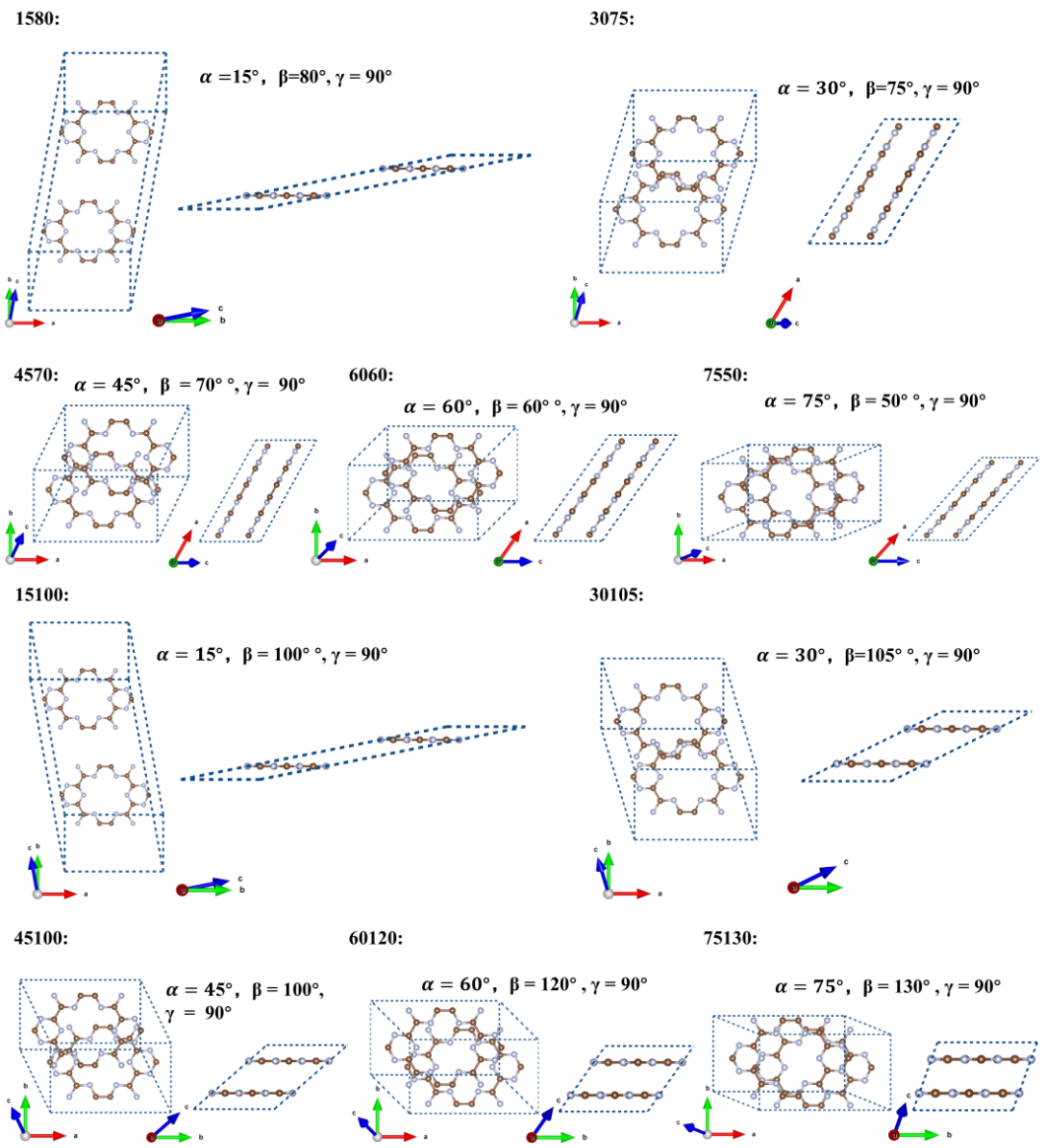

Fig. S4 Different configuration of vdW-CN with different periodic AA' stacking. The dash lines indicate the lattice boundary of the 3D structure cell here.

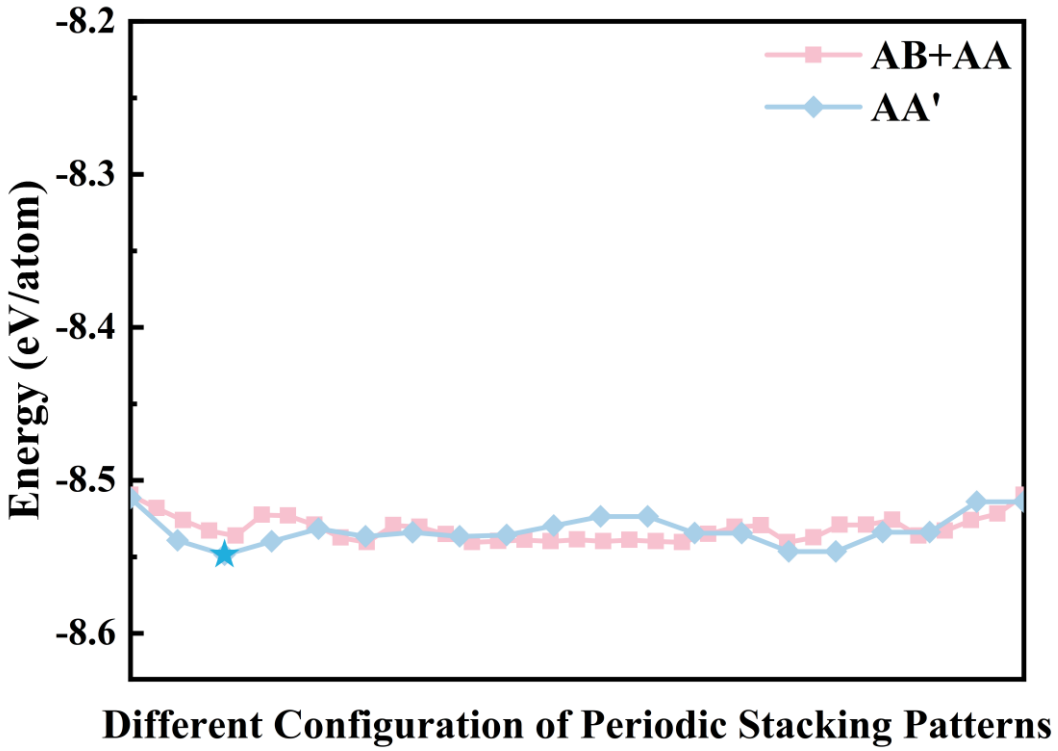

Fig. S5 Structural energy comparison diagram of the three different stacking configurations (AB, AA, and AA') of the vdW-CN structure. A deep blue pentagram marks the lowest energy point.

The thermal stability of vdW-CN

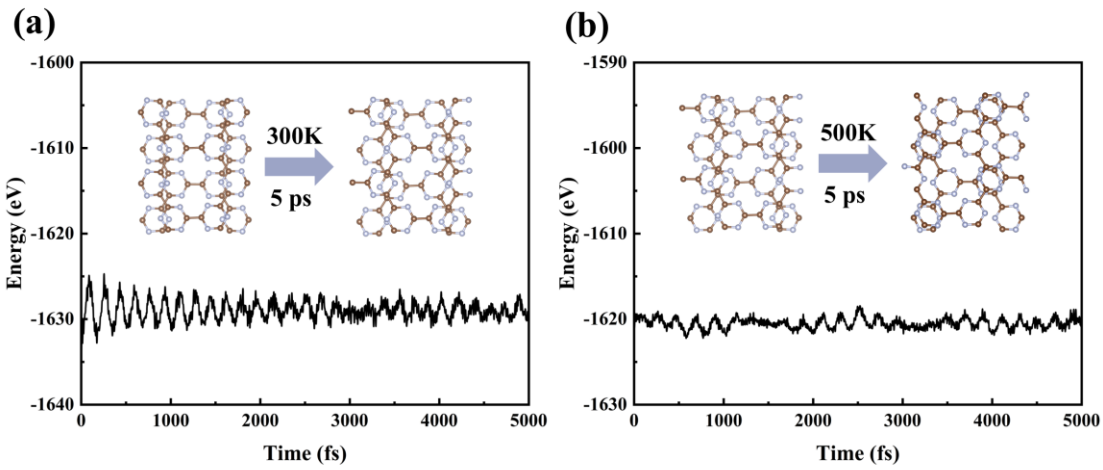

Fig. S6 Ab initio molecular dynamics of the vdW-CN. The energy change during the AIMD simulation process at temperatures of 300 K (a), and 500 K (b), respectively; the snapshots of the vdW-CN supercell structure (1 × 2 × 2) at the end of each stage are inserted in the Figure.

Electronic Properties of vdW-CN Stacked Structures

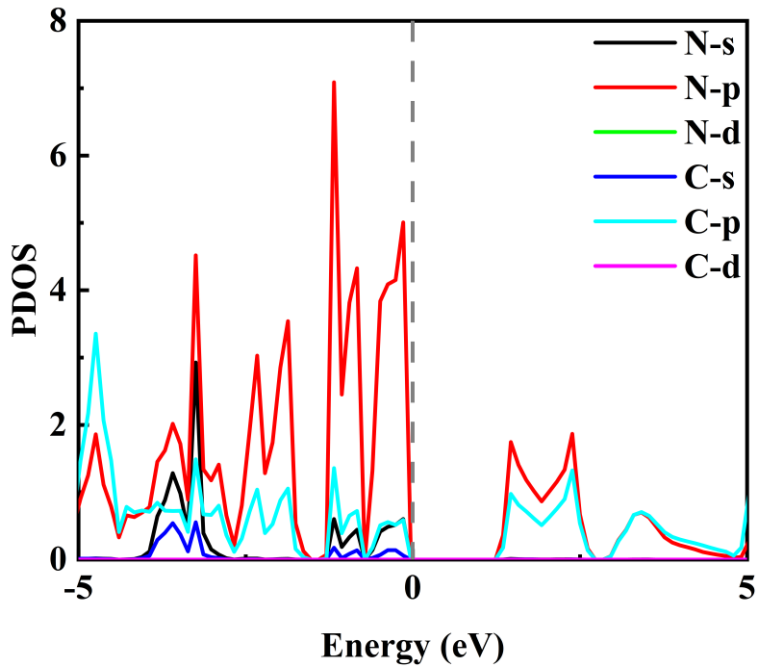

Fig. S7 PDOS of vdW-CN bulk structure unit cell.

Intercalation behaviors of K/Na/Ca Ions in vdW-CN

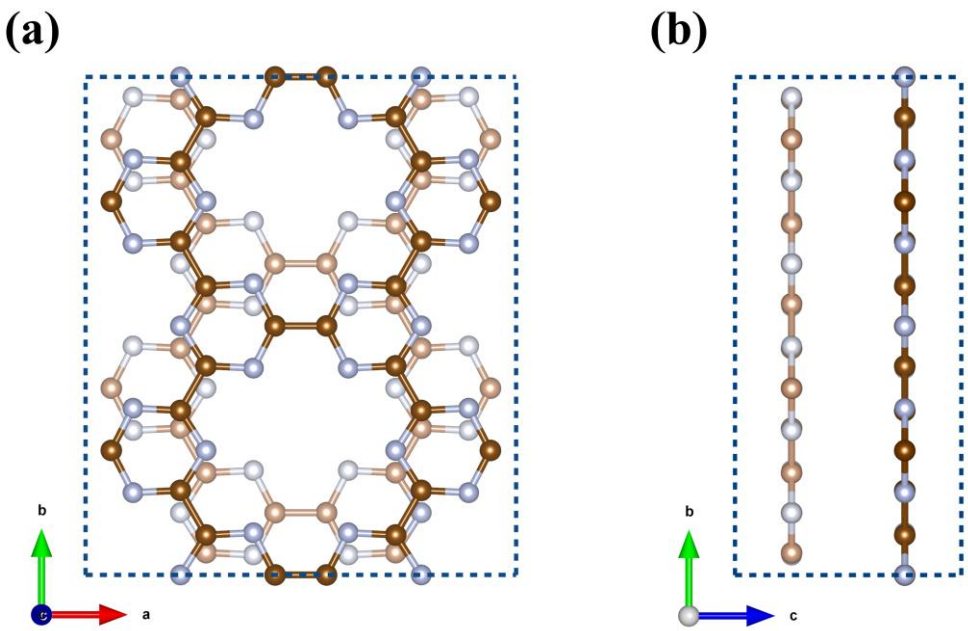

Fig. S8 Top (a) and side (b) view of 2×2×2 supercell of vdW-CN bulk-phase unit cell. The dash lines indicate the lattice boundary of the 3D structure cell here.

The test results indicate that the per-atom energy of a single K/Na atom intercalated into the AB stacking configuration is lower than that of the AA′ stacking configuration, as shown in Fig. S7. Due to the significant intercalation energy of single K/Na/Ca atoms, even a low ratio of ion intercalation ($M_{1/8}C_6N_6$) efficiently induces a transition to AB stacking in the framework structure. Given the similar sizes of sodium and calcium ions, the test results for calcium ions can be referenced from those of sodium ions.

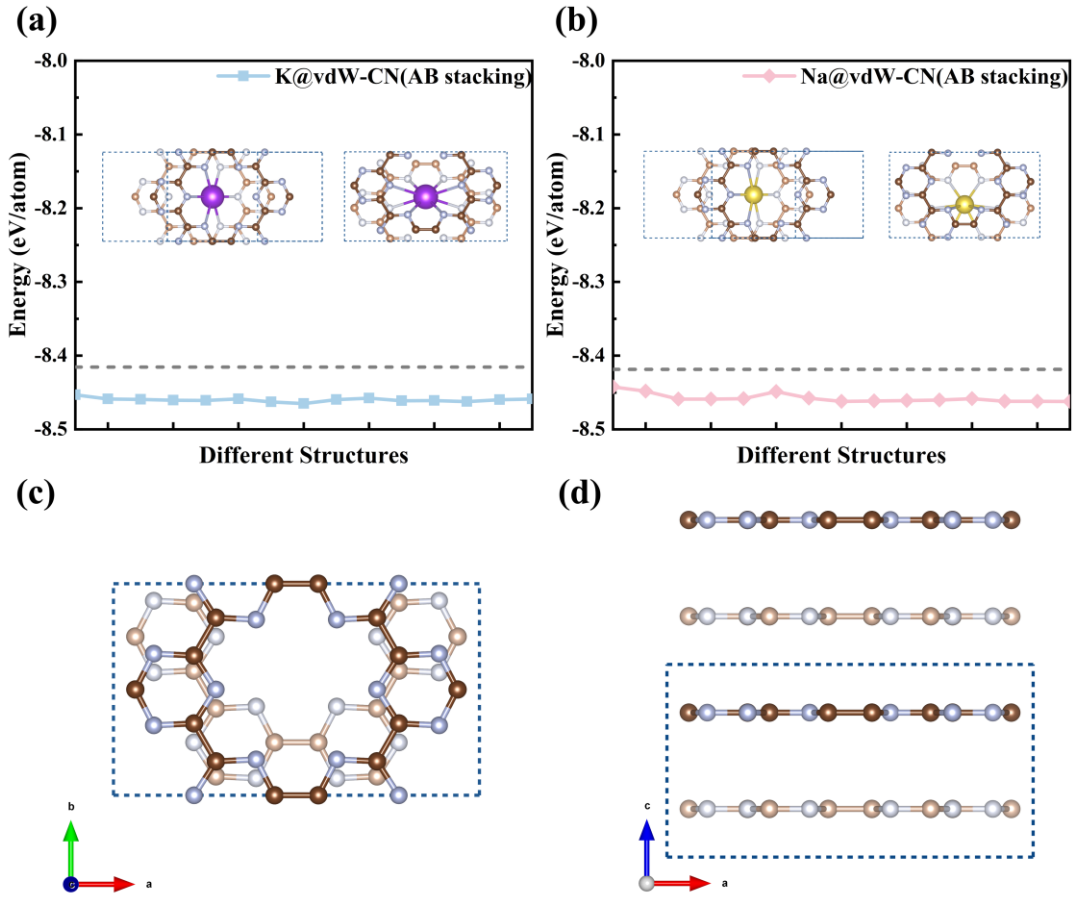

Fig. S9 The per-atom energy comparison diagrams for different AB stacking configurations with a single K/Na ion intercalated (a) and (b). The gray dashed line represents the per-atom energy of the lowest-energy AA′ stacking configuration with a single K/Na ion intercalated. The insets display the top view of the lowest-energy AA′ stacking configuration and the top view of the lowest-energy AB stacking configuration after intercalating a single K/Na ion, respectively. Carbon and nitrogen atoms in

different layers are represented by balls with varying shades of brown and gray, respectively. Top (c) and side (d) view of AB stacking configuration. The dash lines indicate the lattice boundary of the 3D structure cell here.

Migration pathways

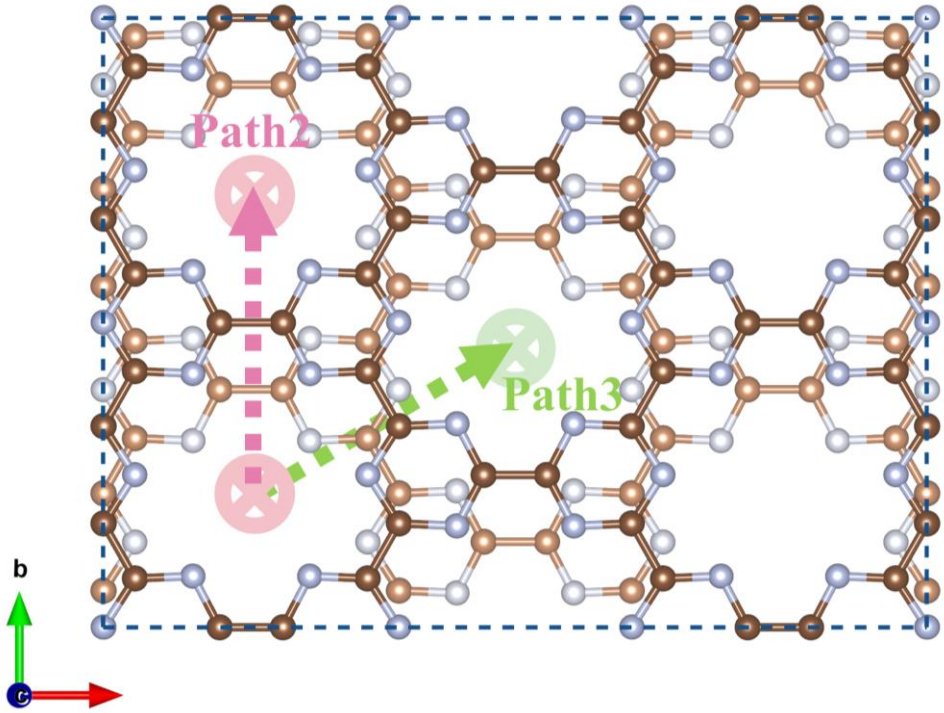

Fig. S10 Migration pathways Path-2 and Path-3 of K/Na/Ca ions along the b and diagonal directions of the ab plane in vdw-CN, respectively. The dash lines indicate the lattice boundary of the 3D structure cell here.

Thermodynamically stable $M_xC_6N_6$ structure

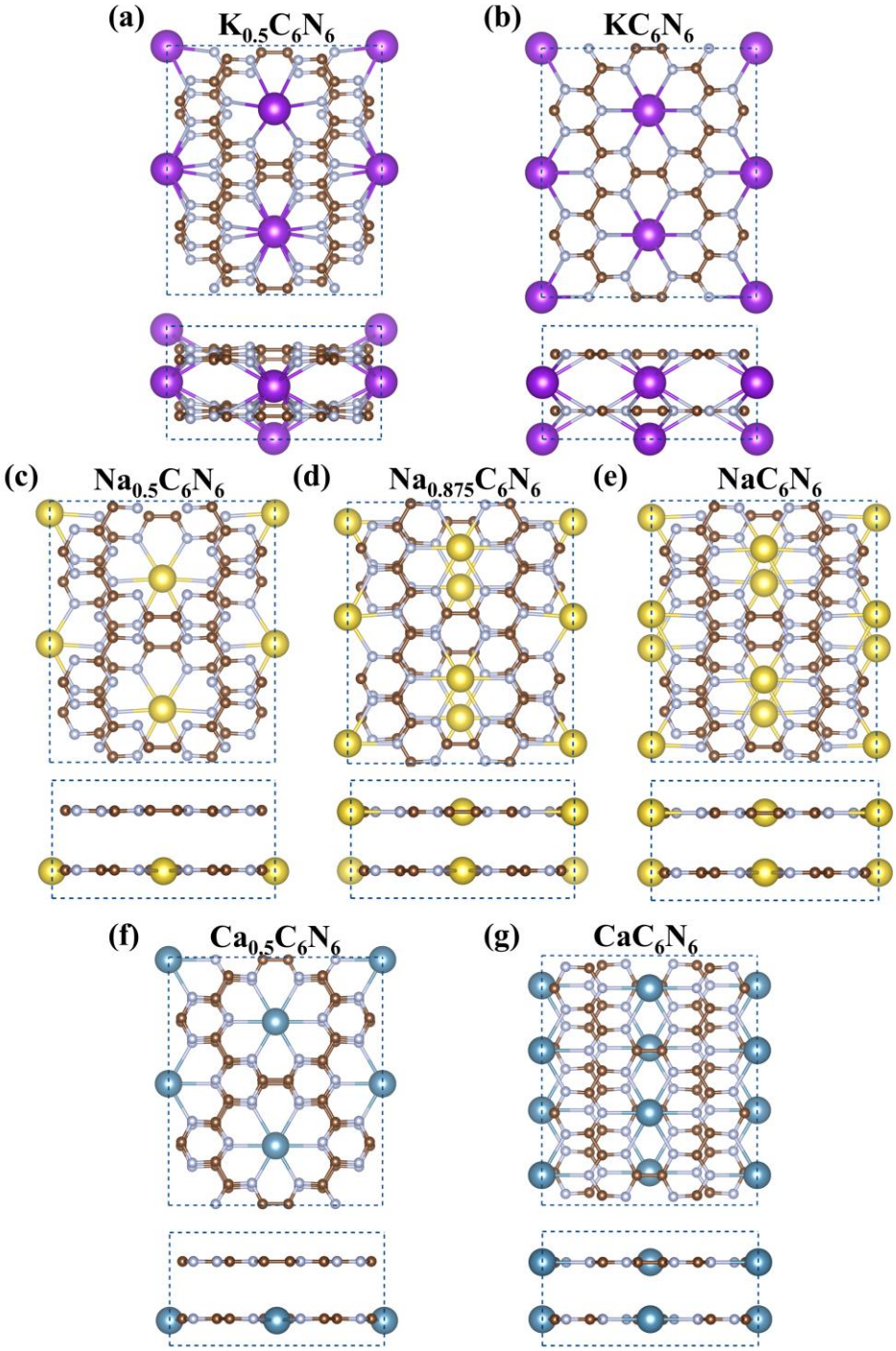

Fig. S11 (a), (b), (c), (e), (f), (g), and (h) correspond to the top and side views of the thermodynamically stable $M_xC_6N_6$ (M=K, Na, Ca) structure, respectively. The dash lines indicate the lattice boundary of the 3D structure cell here.

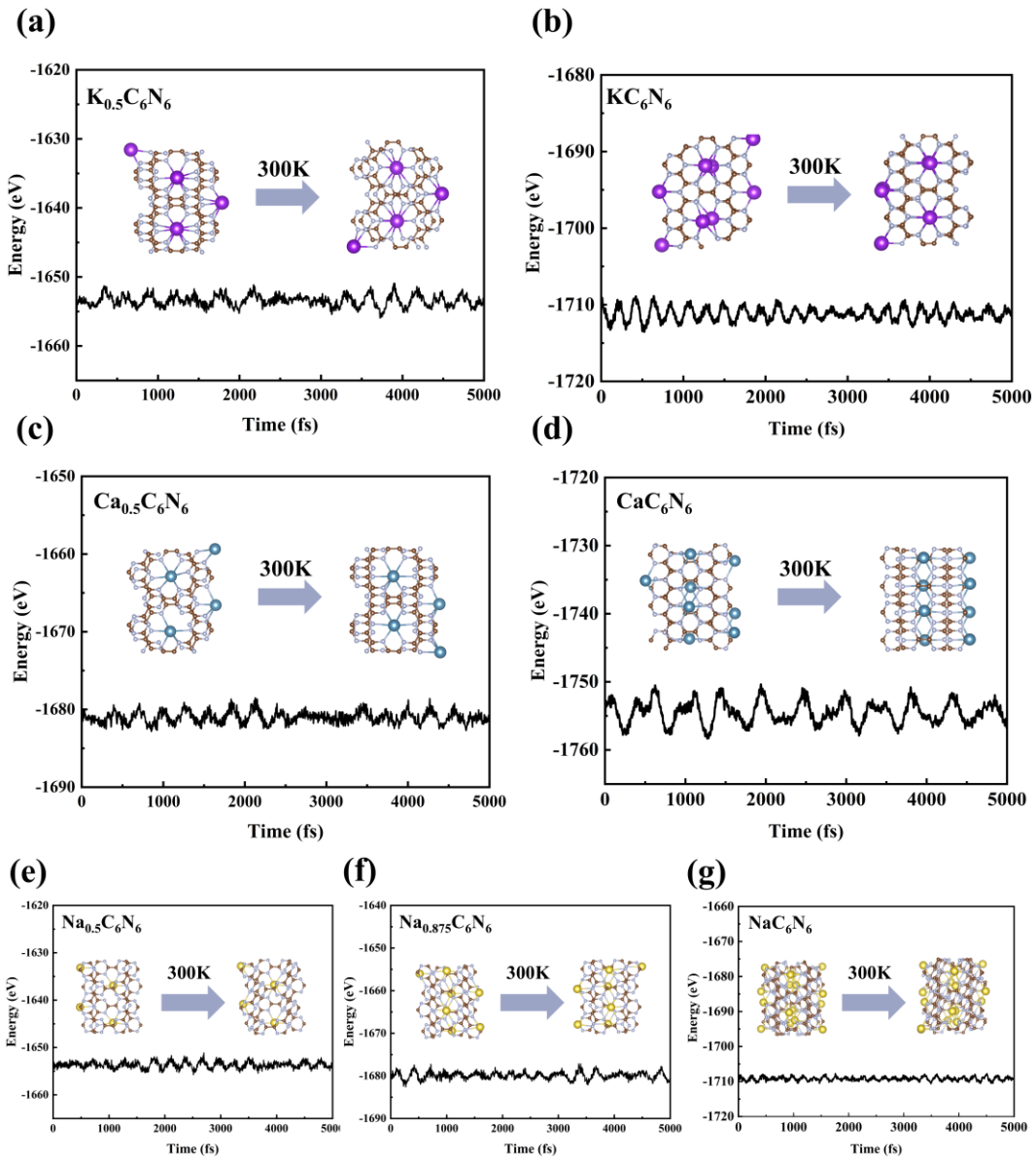

Fig. S12 Ab initio molecular dynamics of thermodynamically stable $K_{0.5}C_6N_6$(a), KC_6N_6(b), $Na_{0.5}C_6N_6$(c), $Na_{0.875}C_6N_6$(d), NaC_6N_6(e), $Ca_{0.5}C_6N_6$(f), and CaC_6N_6(g), respectively. The energy change during the AIMD simulation process at temperatures of 300 K; Top and side views of the configurations at the end of each stage are inserted in the Figure.

The thermal stability of MC_6N_6

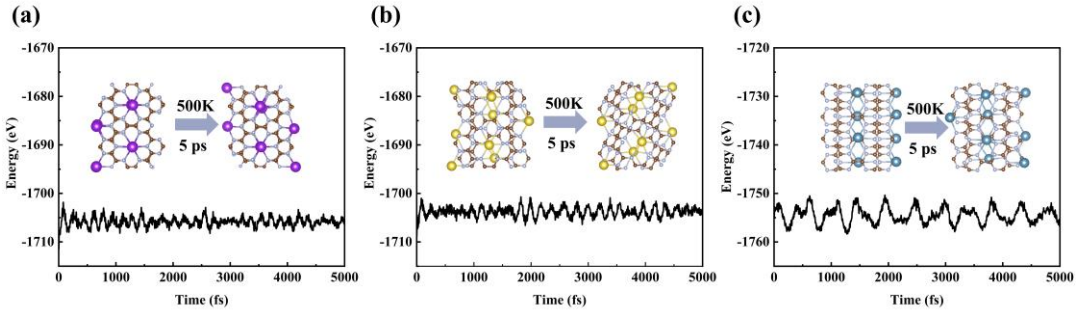

Fig. S13 Ab initio molecular dynamics of the fully inserted configurations KC_6N_6(a), NaC_6N_6(b), and CaC_6N_6(c), respectively. The energy change during the AIMD simulation process at temperatures of 500 K; Top and side views of the fully inserted configurations of K/Na/Ca in vdW-CN at the end of each stage are inserted in the Figure.

The volumetric change rate of $M_xC_6N_6$

Table S1 Volumetric change rate of $Na_xC_6N_6$, $K_xC_6N_6$ and $Ca_xC_6N_6$ (x=0-1) during charging and discharging

Volume change rate (%)	0.25	0.5	0.75	1
K	1.172	-1.308	1.954	-0.660
Na	0.144	-1.263	0.173	0.519
Ca	-0.394	-2.973	-3.265	0.336

Benchmarking table

Table S2 Comparison of vdW-CN as cathode material for K/Na/Ca-ion batteries with other cathode materials. Scalability: ★=Low, ★★=Medium, ★★★=High; Environmental impact: ●=Low, ●●=Medium, ●●●=High.

Cathode materials	Specific capacity [mAh·g^{-1}]	Energy density [Wh·kg^{-1}]	Voltage [V]	scalability	environmental impact
PIBs					
vdW-CN	137	506.1	3.8-3.6	★★★	●
$K_{1.75}Mn[Fe^{II}(CN)_6]_{0.93}$[1]	141	536	3.8	★★	●●
$KCoO_2$[2]	60	-	2.0-3.9	★	●●●
$KVPO_4F$[3]	131	-	4.0	★★	●
$K_{1.89}Mn[Fe(CN)_6]_{0.92}$[4]	155	-	3.6–4.0	★★	●●
P3-$K_{0.5}[Mn_{0.85}Ni_{0.1}Co_{0.05}]O_2$[1]	120	-	1.5-3.9	★★	●●●
$K_2VOP_2O_7$[5]	84	-	3.6	★	●
P′2-$K_x[Ni_{0.05}Mn_{0.95}]O_2$[6]	155	420	1.5-4.3	★★★	●●
$K_3V_2(PO_4)_2F_3$[7]	100	400	3.7	★★	●
$K_{0.220}Fe[Fe(CN)_6]_{0.805}$[7]	73	-	3.1-3.4	★	●●●
SIBs					
vdW-CN	150	470.8	3.3-3.0	★★★	●
$NaFePO_4$[8]	147		1.7	★★	●●
P2-$Na_x[Fe_{1/2}Mn_{1/2}]O_2$[9]	190	520	2.75	★★★	●
β-$NaMnO_2$[10]	191	-	2.7-3.8	★★	●●●
$Na_4MnCr(PO_4)_3$[11]	161	567	3.53	★★	●●
P2-$Na_{0.67}Mn_{0.5}Fe_{0.5}O_2$[9]	190	520	1.5-4.2	★★★	●●
$Na_xK_{0.065}MnO_2$[12]	240	654	-	★★	●●●
CIBs					
vdW-CN	273	847.3	3.4-2.8	★★★	●
α-MoO_3[13]	165	-	2.7	★	●●●
$VOPO_4$[14]	135	-	2.8	★★	●●
$KFe^{3+}(Fe^{2+}(CN)_6)$[15]	165	-	1.07	★	●●●
$Ca_xNa_{0.5}VPO_{4.8}F_{0.7}$[16]	87	-	3.2	★★	●
$NaV_2(PO_4)_2F_3$[17]	110	342	3.5	★★	●●

References

1. X. Bie, K. Kubota, T. Hosaka, K. Chihara and S. Komaba, A novel K-ion battery: hexacyanoferrate(ii)/graphite cell, *J. Mater. Chem. A*, 2017, 5, 4325-4330.
2. Y. Hironaka, K. Kubota and S. Komaba, P2- and P3-K_xCoO_2 as an electrochemical potassium intercalation host, *Chem. Commun*, 2017, 53, 3693-3696.
3. K. Chihara, A. Katogi, K. Kubota and S. Komaba, $KVPO_4F$ and $KVOPO_4$ toward 4 volt-class potassium-ion batteries, *Chem. Commun*, 2017, 53, 5208-5211.
4. L. Xue, Y. Li, H. Gao, W. Zhou, X. Lü, W. Kaveevivitchai, A. Manthiram and J. B. Goodenough, Low-Cost High-Energy Potassium Cathode, *J. Am. Chem. Soc.*, 2017, 139, 2164-2167.
5. H. He, K. Cao, S. Zeng, J. Si, Y. Zhu and C.-H. Chen, $K_2VOP_2O_7$ as a novel high-voltage cathode material for potassium ion batteries, *J. Power Sources*, 2023, 587, 233715.
6. J. U. Choi, Y. Ji Park, J. H. Jo, Y. H. Jung, D.-C. Ahn, T.-Y. Jeon, K.-S. Lee, H. Kim, S. Lee, J. Kim and S.-T. Myung, An optimized approach toward high energy density cathode material for K-ion batteries, *Energy Storage Mater.*, 2020, 27, 342-351.
7. C. Zhang, Y. Xu, M. Zhou, L. Liang, H. Dong, M. Wu, Y. Yang and Y. Lei, Potassium Prussian Blue Nanoparticles: A Low-Cost Cathode Material for Potassium-Ion Batteries, *Adv. Funct. Mater.*, 2017, 27, 1604307.
8. K. Zaghib, J. Trottier, P. Hovington, F. Brochu, A. Guerfi, A. Mauger and C. M. Julien, Characterization of Na-based phosphate as electrode materials for electrochemical cells, *J. Power Sources*, 2011, 196, 9612-9617.
9. N. Yabuuchi, M. Kajiyama, J. Iwatate, H. Nishikawa, S. Hitomi, R. Okuyama, R. Usui, Y. Yamada and S. Komaba, P2-type $Na_x[Fe_{1/2}Mn_{1/2}]O_2$ made from earth-abundant elements for rechargeable Na batteries, *Nat. Mater.*, 2012, 11, 512-517.
10. J. Billaud, R. J. Clément, A. R. Armstrong, J. Canales-Vázquez, P. Rozier, C. P. Grey and P. G. Bruce, β-$NaMnO_2$: A High-Performance Cathode for Sodium-Ion Batteries, *J. Am. Chem. Soc.*, 2014, 136, 17243-17248.
11. J. Zhang, Y. Liu, X. Zhao, L. He, H. Liu, Y. Song, S. Sun, Q. Li, X. Xing and J. Chen, A Novel NASICON-Type $Na_4MnCr(PO_4)_3$ Demonstrating the Energy Density Record of Phosphate Cathodes for Sodium-Ion Batteries, *Adv. Mater.*, 2020, 32, 1906348.
12. C. Wang, L. Liu, S. Zhao, Y. Liu, Y. Yang, H. Yu, S. Lee, G.-H. Lee, Y.-M. Kang, R. Liu, F. Li and J. Chen, Tuning local chemistry of P2 layered-oxide cathode for high energy and long cycles of sodium-ion battery, *Nat. Commun.*, 2021, 12, 2256.
13. S. Kim, L. Yin, S.-M. Bak, T. T. Fister, H. Park, P. Parajuli, J. Gim, Z. Yang, R. F. Klie, P. Zapol, Y. Du, S. H. Lapidus and J. T. Vaughey, Investigation of Ca Insertion into α-MoO_3 Nanoparticles for High Capacity Ca-Ion Cathodes, *Nano Lett.*, 2022, 22, 2228-2235.
14. J. Wang, S. Tan, F. Xiong, R. Yu, P. Wu, L. Cui and Q. An, $VOPO_4 \cdot 2H_2O$ as a new cathode material for rechargeable Ca-ion batteries, *Chem. Commun*, 2020, 56, 3805-3808.
15. N. Kuperman, P. Padigi, G. Goncher, D. Evans, J. Thiebes and R. Solanki, High performance Prussian Blue cathode for nonaqueous Ca-ion intercalation battery, *J. Power Sources*, 2017, 342, 414-418.
16. Z.-L. Xu, J. Park, J. Wang, H. Moon, G. Yoon, J. Lim, Y.-J. Ko, S.-P. Cho, S.-Y. Lee and K. Kang, A new high-voltage calcium intercalation host for ultra-stable and high-power

calcium rechargeable batteries, *Nat. Commun.*, 2021, 12, 3369.

17. C. Chen, F. Shi, S. Zhang, Y. Su and Z.-L. Xu, Ultrastable and High Energy Calcium Rechargeable Batteries Enabled by Calcium Intercalation in a NASICON Cathode, *Small*, 2022, 18, 2107853.